ChemPubSoc Europe

DOI: 10.1002/cptc.201800150

CHEMPHOTOCHEM Articles

Highly Efficient Energy Transfer Cassettes by Assembly of Boronic Acid Derived Salicylidenehydrazone Complexes

Fábio M. F. Santos,[a] Zoe Domínguez,[b] María M. Alcaide,[b, c] Ana I. Matos,[a] Helena F. Florindo,[a] Nuno R. Candeias,[d] Pedro M. P. Gois,*[a] and Uwe Pischel*[b]

Energy transfer cassettes that build on the platform of boronic acid derived salicylidenehydrazone (BASHY) complexes were prepared. The functional flexibility of the BASHY chromophore was underpinned by its tunable role as energy donor or acceptor, integrated in compact and non-conjugated bichromophoric dyads. The energy transfer is highly efficient ($\Phi_{ET} > 0.95$) and is assumed to proceed mainly via a through-bond mechanism. Both constituent chromophores benefit mutually from their integration in the cassettes: a) The pseudo Stokes shift is increased to 110–200 nm; b) the antenna (donor) chromophore improves the light absorption of the acceptor chromophore; and c) the emission window of the BASHY chromophore is expanded in the BASHY-Bodipy dye without using strategies that compromise the observation of high quantum yields. The application of the cassettes for the formulation of fluorescent polymeric nanoparticles, that can be internalized in cells and observed by fluorescence imaging, was demonstrated using the BASHY-Bodipy dye as an example.

1. Introduction

Multicomponent reactions are versatile procedures for the synthesis of heterocyclic skeletons with variable substitution patterns.[1–5] Recently dye chemists have started to realize the potential of this tool for the discovery of new fluorophore platforms or for the extension of known fluorophore families with functional handles.[5–7] Principally two approaches are distinguished:[5] (a) the "scaffold approach" with at least one of the reactants already containing a dye and (b) the "chromophore approach", where the dye is actually formed during the reaction. This yields the expansion of chemical space with previously unknown fluorophores and their property-driven optimization for applications in bioimaging and sensing.[8–14] Our groups have contributed to this trend of dye chemistry with the development of the synthetically and functionally flexible BASHY (boronic acid derived salicylidenehydrazone complexes) dye platform.[15–17] This one builds on straightforward multicomponent condensation reactions, implying salicylidenehydrazones and boronic acids. These dyes were shown to have application potential in bioimaging.[15,18,19]

An interesting facet of the photophysical engineering of fluorophores is their integration into energy transfer cassettes (ETC).[20–25] Such constructs combine an energy donor dye with an acceptor dye to allow highly efficient energy transfer communication between both entities, involving through-space and/or through-bound mechanisms. This strategy enables the photophysical improvement of the dyes to arrive at increased pseudo Stokes shifts (spectral separation of absorption and fluorescence bands) and efficient light absorption/emission, i.e. high brightness. Both characteristics are important technical assets for applications of dyes in bio-relevant contexts.[26] For example, ETC have found use in sensing,[24,25,27] in fluorescence microscopy,[24,28–30] in lasing applications,[31,32] for multicolor labeling,[33] and in theranostic logic devices.[34,35] The donor-acceptor linkage is often realized by employing metal-catalyzed coupling reactions (e.g., Cu-catalyzed click reaction, Pd-catalyzed Sonogashira coupling). However, these methods generally require the implementation of laborious purification protocols, as already traces of the metal catalyst in the final product may for example cause undesired fluorescence quenching. Hence, the development of metal-free alternatives with extended product scope continues to be an objective in the field.

Herein we describe the convenient preparation of ETC based on the assembly of BASHY dyes using the "chromophore approach" or its combination with the "scaffold approach". The obtained ETC show practically quantitative energy transfer efficiency and integrate variable donor/acceptor scenarios, emphasizing the photophysical flexibility of the BASHY dye platform for the design of such architectures.

[a] F. M. F. Santos, A. I. Matos, Dr. H. F. Florindo, Dr. P. M. P. Gois
Research Institute for Medicines (iMed.ULisboa)
Faculty of Pharmacy
University of Lisbon
Av. Prof. Gama Pinto, 1649-003 Lisbon (Portugal)
E-mail: pedrogois@ff.ulisboa.pt

[b] Z. Domínguez, M. M. Alcaide, Dr. U. Pischel
CIQSO-Center for Research in Sustainable Chemistry and
Department of Chemistry
University of Huelva
Campus de El Carmen s/n, E-21071 Huelva (Spain)
E-mail: uwe.pischel@diq.uhu.es

[c] M. M. Alcaide
Institute for Chemical Research (CSIC-US)
Av. Américo Vespucio 49, E-41092 Seville (Spain)

[d] Dr. N. R. Candeias
Laboratory of Chemistry and Bioengineering
Tampere University of Technology
Korkeakoulunkatu 8, 33101 Tampere (Finland)

Supporting information for this article is available on the WWW under https://doi.org/10.1002/cptc.201800150

2. Results and Discussion

2.1. Synthesis and Photophysical Characterization of BASHY-Bodipy Dye 3

Dye **3** was prepared by the condensation reaction between stoichiometric amounts of the salicylidenehydrazone ligand **1** and a boronic acid modified Bodipy dye (Figure 1a and Experimental Section).[17] Note that as recently discussed by us, for the specific case of *N,N*-dialkylamino-substituted BASHY dyes the reaction is done as a sequential procedure and not as a classical three-component reaction as for other BASHY dyes.[15] Bodipy dyes as acceptor chromophores are a common choice for ETC, due to their favorable absorption properties (large molar absorption coefficients) and high emission quantum yields.[20,21,36,37] Strictly seen, the preparation of dye **3** is a combination of the "chromophore approach" (for the construction of the BASHY chromophore) and the "scaffold approach" (taking into account that the boronic acid component already contains a Bodipy fluorophore; see Figure 1).

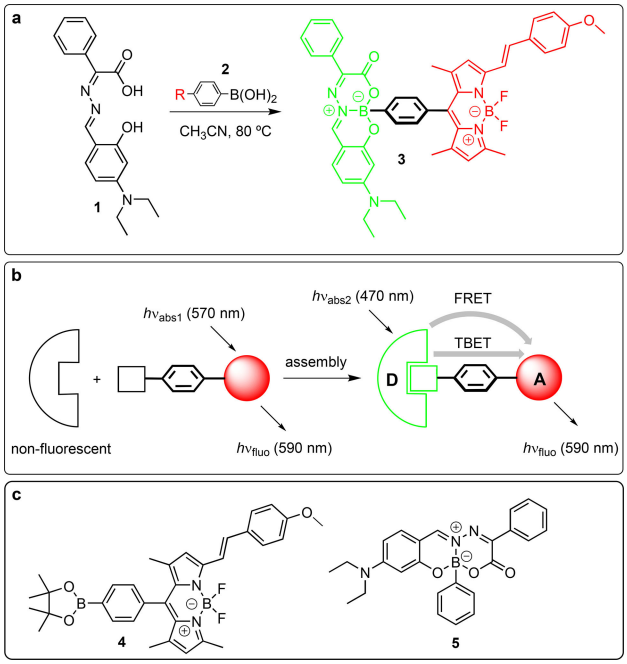

Figure 1. a) Assembly of dye **3**, b) illustration of the approach for the assembly of an energy-transfer cassette, c) structures of the individual chromophores that are integrated in **3**. FRET: Förster resonance energy transfer, TBET: through-bond energy transfer.

Table 1. Photophysical data of the bichromophoric dyes **3** and **7** and the models **4**–**6**.

	$\lambda_{abs,max}$ [nm][a] (ε [$M^{-1}cm^{-1}$])	$\lambda_{fluo,max}$ [nm][b]	$\Delta\nu$ [cm^{-1}][c]	Φ_{fluo}[d]	τ_{fluo} [ns][e]
3[f]	473 (52000) 572 (74000)	582	3990	0.76	3.70
4[f]	574 (75000)	586	340	0.78	4.04
5[f]	471 (63000)	508	1580	0.60	2.38
6[g]	323 (4100)	–	–	–	–
7[g]	320 (13700) 479 (71400)	519	11980	0.69	10.53

[a] Absorption maximum; in parenthesis the corresponding molar absorption coefficient is given. [b] Fluorescence emission maximum. [c] Stokes shift. [d] Fluorescence quantum yield (see Experimental Section); error 15%, excitation in long-wavelength absorption band. [e] Fluorescence lifetime obtained by time-correlated single-photon-counting; 5% error, excitation in long-wavelength absorption band. [f] In toluene. Data for dye **5** are from ref. 15. [g] In chloroform.

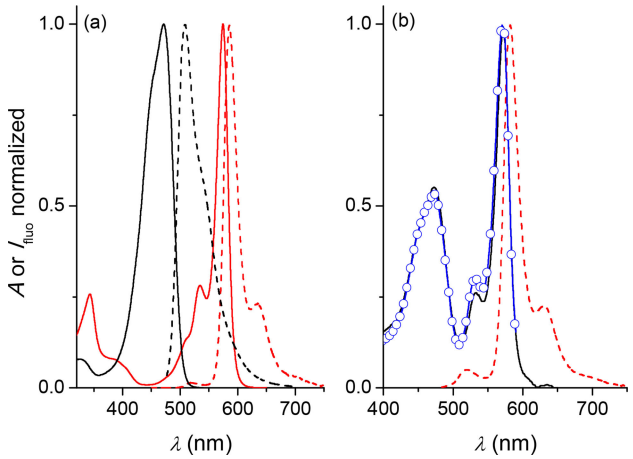

Figure 2. a) UV/Vis absorption (solid lines) and corrected fluorescence spectra (dashed lines) of **4** (red) and **5** (black) in air-equilibrated toluene. b) UV/Vis absorption spectrum (black solid line) and corrected fluorescence spectrum (red dashed line; excitation at 473 nm) of dye **3** in air-equilibrated toluene. In blue the corrected excitation spectrum, monitoring the Bodipy emission (at 615 nm), is shown.

The main photophysical data of the investigated dyes are summarized in Table 1. The BASHY-Bodipy dye **3** has a UV/vis absorption spectrum with the typical strong bands for both chromophore moieties; see Figure 2b: a band with a maximum at 473 nm, corresponding to the BASHY skeleton,[15,17] and a band with a maximum at 572 nm which is characteristic for the styryl-Bodipy chromophore.[36] This observation underlines the fact that the chromophore units are non-conjugated. The BASHY chromophore fills the optical window in the absorption spectrum of the Bodipy chromophore (410–490 nm, where the absorbance is $\leq$5% of the absorbance at the maximum at 572 nm; see Figure 2a for dye **4**), enabling selective excitation and the use of commercial laser sources such as the Ar ion laser (488 nm).

On the one hand, on selective excitation into the Bodipy absorption band ($\lambda_{exc} > 520$ nm) the typical emission of this chromophore with a maximum at 582 nm and with a high quantum yield of $\Phi_{fluo} = 0.76$ was observed. This value compares very nicely with the one of the individual Bodipy chromophore **4** (see Table 1) and rules out significant through-space fluorescence quenching of the Bodipy chromophore by the ground-state BASHY moiety. On the other hand, also the selective excitation of the BASHY chromophore at 473 nm yielded practically only Bodipy emission. The strong quenching of the BASHY fluorescence hints on a quantitative energy transfer ($\Phi_{ET} > 95\%$). This was confirmed by the superposition of the normalized absorption and excitation spectra (monitor-

ing selectively the Bodipy emission) of **3**; see Figure 2b.[38] Due to the rigidity and non-planarity of the dye (see the geometry-optimized structure in the Supporting Information) and the proximity of both chromophores, that are linked by a phenylene spacer (the boron-boron distance is 8.93 Å), the operation of through-bond energy transfer (TBET) is postulated (see Figure 1). TBET is generally observed for ETC architectures, where the donor and acceptor are connected by an unsaturated linker and the whole system is non-planar due to steric hindrance.[20,27] However, two additional observations are worth being noted. First, the orbital overlap at the chromophore-linker connection is close to zero, because the linker assumes a perpendicular orientation with respect to both chromophore planes (see Figure 3 and Supporting Information). This excludes

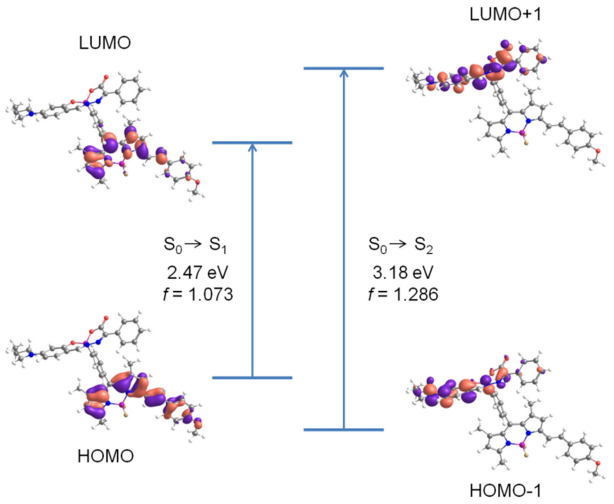

Figure 3. Contour plots of the main frontier orbitals involved in the first two electronic transitions in dye **3**.

Dexter exchange energy transfer,[39,40] as discussed for a series of ETC with similar geometrical conditions.[21,41] However, it should be emphasized that Dexter-type exchange is not the only contributor to the TBET mechanism. Second, Förster resonance energy transfer (FRET)[40,42] is likely to operate in parallel to TBET.[27] This is corroborated by the considerable spectral overlap ($J = 1.6 \times 10^{-10}$ cm^6 mol^{-1}) between the efficient donor emission and the strong acceptor absorption (see Figure 2a, dashed black and solid red spectra), the non-perpendicular orientation of the donor and acceptor transition dipole moments, and the short inter-chromophore distance. The critical Förster radius is calculated as $R_0 = 47$ Å, far larger than the actual boron-boron distance in **3** (see above). Would FRET be the only energy transfer pathway, then this alone would yield an efficiency of practically 100%. However, as mentioned above, it is very likely that TBET competes with FRET and the quantitative energy transfer is partitioned between both pathways.

Noteworthy, the integration of both chromophores in the ETC results in their mutual improvement. (a) The Bodipy chromophore can be excited now in the optical window between 410 nm and 490 nm, taking advantage of BASHY as an antenna. (b) The pseudo-Stokes shift is considerably increased from 10 nm to *ca.* 120 nm (in absolute energy units: 340 cm^{-1} to 3990 cm^{-1}). (c) The fluorescence output, obtained on excitation of BASHY, can be further red-shifted in comparison to the individual BASHY chromophore. In theory, such red-shift could be also achieved by increasing the charge-transfer character of the BASHY skeleton.[15,17] However, a reduced fluorescence quantum yield, as direct consequence of the energy-gap law, applies to such electronic fine-tuning.[15] Finally, it should be commented that BASHY dyes are very photostable during extended irradiation with a 150 W Xe lamp, as has been shown for a large pool of these dyes with variable substitution patterns.[15,17]

2.2. Time-Dependent Density-Functional-Theory (TD-DFT) Calculations with Dye 3

The CAM-B3LYP functional[43] and a 6-31G** basis set were employed and toluene was included as solvent by means of the application of the polarization continuum model (PCM).[44] In Figure 3 the frontier orbitals that are implicated in the first two transitions, $S_0 \rightarrow S_1$ and $S_0 \rightarrow S_2$, are shown. On the one hand, the lowest energy excitation ($S_0 \rightarrow S_1$) involves mainly the HOMO→LUMO transition with the frontier orbitals being exclusively located on the Bodipy chromophore. On the other hand, the energetically higher lying $S_0 \rightarrow S_2$ excitation includes the HOMO-1→LUMO+1 transition. These orbitals are localized on the BASHY moiety. For both chromophores the highest occupied orbitals (HOMO and HOMO-1) include the respective electron donor unit: the *p*-MeO-phenyl for the Bodipy and the Et_2N-phenyl for the BASHY. The lowest unoccupied orbitals are moved away from the electron donors, being located on the Bodipy heterocycle (LUMO) or moved along the boron salicylidenehydrazone backbone (LUMO+1). These observations emphasize the push-pull character of both chromophoric units.

Another important information comes from the ground-state optimized structure of **3**. The electronic separation of BASHY and Bodipy is evident by the perpendicular alignment of the connecting phenylene linker with respect to both chromophores (see Supporting Information). This sterically induced twist hinders the π-conjugative electronic communication between the two dye moieties, thereby defining **3** as a cassette architecture. Similar observations have been made for other ETC, among them those containing Bodipy chromophores.[20,21,23,25,31,32,45]

2.3. Use of Dye 3 in Bioimaging

ETC find often application in bioimaging.[28,29,46] As a case of example we decided to prepare biocompatible polymeric PLGA/PVA [poly (lactide-co-glycolide)/poly (vinyl alcohol)] nanoparticles (NP) (mean size 219±4 nm, polydispersity index 0.112±0.005, zeta potential −0.88±0.15), loaded with dye **3**,

by using a double emulsion (*water-in-oil-in-water*: *w/o/w*) solvent evaporation method.[47] This formulation bears two advantages, as recently discussed:[15] (a) encapsulated BASHY chromophores are expected to be more stable against hydrolytic degradation and (b) the nonpolar environment that is created by the NPs triggers the BASHY chromophores to be inherently more fluorescent, being an advantage for their performance in ETC. The dye-loaded NP were then incubated with murine immature bone marrow dendritic cells (BMDC, JAW SII, ATCC®CRL-11904™) for 1, 3, and 18 h to assess NP internalization and the impact on cell viability by flow cytometry. The BMDC internalization levels (98–100% positive cells) obtained for the free dye **3** were similar to those observed for dye-loaded NP, 18 h after incubation. At shorter incubation times (1 and 3 h) the internalization levels (%) obtained for dye-loaded NP were lower (63 and 88%) than those observed for the free dye **3** (Figure 4a). This time-dependent internalization profile was

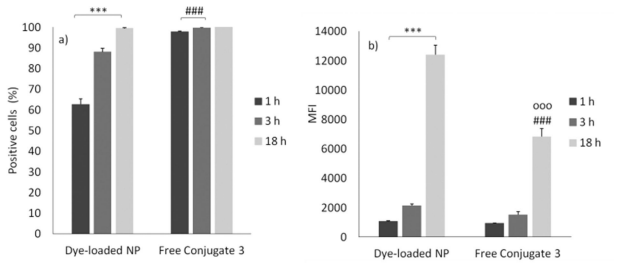

Figure 4. Internalization of free dye **3** (2.5 μg mL^{-1}) and dye-loaded NP (0.5 mg mL^{-1}) by BMDC (JAW SII, ATCC®CRL-11904™), after 1, 3, and 18 h of incubation, expressed by a) percentage and b) median fluorescence intensity (MFI) of positive cells in the population sorted by the flow cytometer (mean ± SD; $N = 3$; $n = 2$). Statistics: two-way ANOVA and Tukey's post-hoc test. For all incubation time points $^{***}p < 0.001$; relative to dye-loaded NP, for the respective incubation time point $^{###}p < 0.001$; and relative to lower incubation time points, for free dye **3** $^{ooo}p < 0.001$.

expected for NP, having in consideration the nanoparticulate nature of this carrier *versus* the molecular structure of the free dye explored in this study.

Noteworthy, the median fluorescence intensity (MFI) values evidence that the dye-loaded NP were internalized at higher extent than the free dye **3** (Figure 4b). The free dye **3** and the dye-loaded NP did not have a negative impact on the viability of BMDC up to 18 h of incubation, as determined by the propidium iodide (PI) assay (Figure 5).

Confocal fluorescence microscopy (Figure 6) analysis confirmed the successful internalization of dye-loaded NP by BMDC after 2, 4 and 10 h of incubation. The dye-loaded NP were conveniently and selectively excited at 488 nm (Ar ion laser) and a bright fluorescence signal was detected at 580 nm.

BASHY dyes can be designed with high functional modularity and offer photophysical properties such as high molar absorption coefficients (*ca.* 60000 M^{-1}cm^{-1}) and high emission quantum yields (*ca.* 0.5–0.6).[15,17] This makes these dyes very interesting antenna chromophores in ETC, such as the investigated dye **3** and especially the dye-loaded NP version. As regards the free dye, the preferential accumulation and light-up

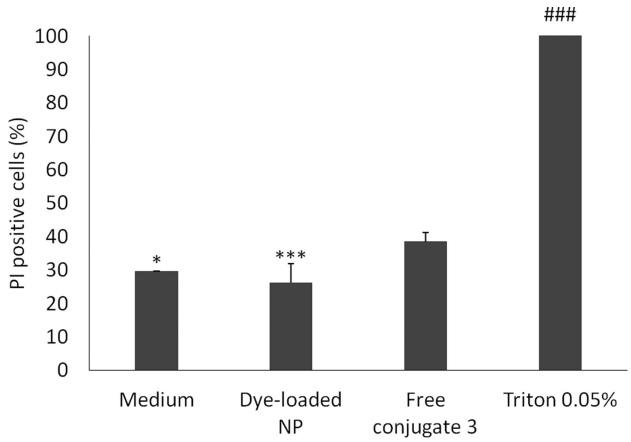

Figure 5. Impact of dye **3**, free and loaded in NP, on BMDC (JAW SII, ATCC®CRL-11904TM) viability. The population of dead cells was determined with the propidium iodide (PI) assay 18 h post-incubation with free dye **3** (2.5 μg mL^{-1}) and dye-loaded NP (0.5 mg mL^{-1}), being expressed as the percentage of PI positive cells in the population; sorted by flow cytometry (mean ± SD; $N = 3$; $n = 2$). Statistics: one-way ANOVA and Tukey's post-hoc test. Relative to free dye **3** $^{*}p < 0.05$ and $^{***}p < 0.001$; and relative to medium, to dye **3**, and dye-loaded NP $^{###}p < 0.001$.

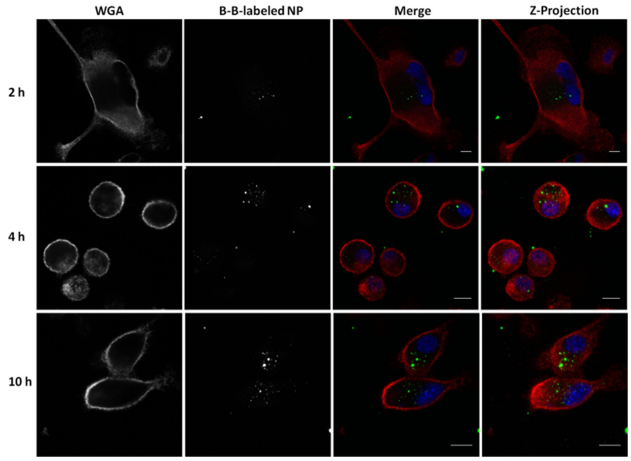

Figure 6. Confocal microscopy images obtained after incubation of BMDC (JAW SII, ATCC®CRL-11904TM) with **3**-loaded NP (B-B-labeled NP, 0.5 mg mL^{-1}, green), for 2, 4 and 10 h. Nuclei and plasma membrane were stained with Hoechst 33342 (2 μg mL^{-1}, blue) and WGA-Alexa Fluor 633 (5 μg mL^{-1}, red), respectively. Representative images of two independent experiments are shown. Scale bars = 10 μm.

behavior of the BASHY motif in lipidic cellular substructures implies an interesting potential of the ETC as selective bioimaging probes.[15]

2.4. Synthesis and Photophysical Characterization of BASHY-Bodipy Dye 7

With the idea to demonstrate the photophysical flexibility of our approach we aimed at the design of an ETC architecture where the BASHY chromophore would play the role of the energy acceptor instead. Based on photophysical rationales and previous reports of other coumarin-containing ETC architec-

tures[32,45,48,49] we predicted that the combination of the BASHY chromophore with a coumarin would serve this objective (see Figure 7). We synthesized dye **7** in an analogous way as **3**, using

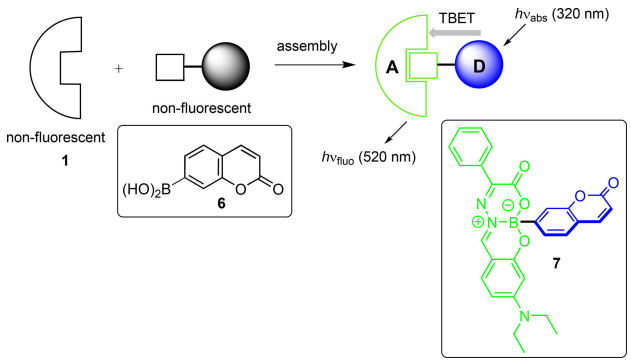

Figure 7. Assembly of dye **7** from ligand **1** and coumarinylboronic acid **6** and energy transfer process in **7**.

ligand **1** and the coumarinylboronic acid **6**; see Experimental Section. This allowed a very compact arrangement of both fluorophores in the final ETC, just being separated by a single σ-bond. The concrete example is a clear representation of the "chromophore approach", as dye **7** is entirely constructed from the non-fluorescent building blocks **1** and **6** (see below).

For the reason of a better optical transparency below 300 nm chloroform was preferred over toluene for the corresponding experimental photophysical studies (key data in Table 1; see above). The UV/vis absorption spectrum of dye **7** shows the feature of the coumarin chromophore with maxima at 282 nm and 320 nm and the BASHY absorption band with a maximum at 479 nm; see Figure 8. On selective excitation into

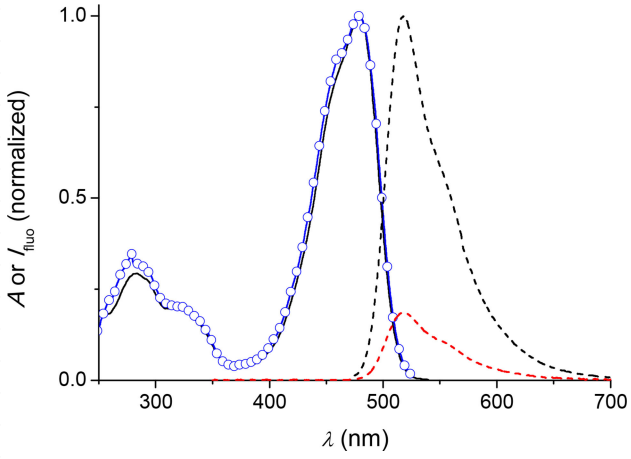

Figure 8. UV/Vis absorption (black solid line) and corrected fluorescence spectra for excitation at 320 nm (red dashed line) and 470 nm (black dashed line) of dye **7** in air-equilibrated chloroform. Note that the red emission spectrum is less intense due to the smaller light absorption at 320 nm as compared to 470 nm. The blue spectrum corresponds to the corrected excitation spectrum monitoring the BASHY emission (at 550 nm).

the BASHY absorption band the typical strong green fluorescence ($\lambda_{fluo,max}$ = 519 nm in chloroform) of this chromophore was detected. On excitation into the coumarin band at 320 nm the same highly efficient BASHY emission was seen. Noteworthy, no coumarin fluorescence was observed. The ultimate proof for a practically quantitative energy-transfer process ($\Phi_{ET} > 0.95$) comes from the superposition of the corresponding excitation spectrum, monitoring the BASHY fluorescence, and the absorption spectrum of the dye; see Figure 8.[38] Very clearly the absorption characteristics of the coumarin in the region between 270 and 340 nm are completely reproduced in the excitation spectrum. The presence of the coumarin antenna effectively leads to an increased pseudo Stokes shift of *ca.* 200 nm *versus ca.* 50 nm for the direct excitation into the BASHY chromophore absorption band (11980 cm^{-1} *versus* 1870 cm^{-1} in absolute energy).

Noteworthy, the coumarinylboronic acid **6**, being the precursor for the formation of the BASHY skeleton, is non-fluorescent. Such a situation speaks in principle against the operation of FRET.[50] However, the integration of **6** into the BASHY chromophore triggers the *Umpolung* of the electron-accepting $B(OH)_2$ into an electron-donating BO_2N^-, thereby possibly activating the fluorescence of the coumarin itself (i.e., in absence of an energy acceptor), as observed for other electron-donating groups in the 7-position, e.g., *N,N*-dialkylamino or methoxy.[51,52] In any case, given the non-fluorescent nature of the model compound **6** no FRET data in form of the spectral overlap integral and critical radius could be estimated. However, while the FRET mechanism cannot be conclusively discussed, it is very reasonable to assume that TBET is indeed operative in dye **7**, integrating both chromophores very compactly and at a minimal distance of one single bond. It should be noted that contrary to FRET the TBET mechanism does not require spectral overlap.[20,27] The cassette-like behavior of **7**, and hence the operation of the through-bond mechanism, is confirmed by similar calculations (CAM-B3LYP/6-31G**) as discussed above for dye **3**; see Supporting Information for details.

3. Conclusions

In conclusion, building on the assembly of the BASHY chromophore, two highly efficiently and compact (i.e., geometrically very defined) ETC, where the BASHY plays either the role of the energy donor (dye **3**) or the energy acceptor (dye **7**), were realized. These are the first examples for the integration of BASHY into through-bond ETC. The construction of these photofunctional architectures was possible by implementing the "chromophore approach" or its combination with the "scaffold approach" in straightforward condensation reactions between boronic acid derivatives and a salicylidenehydrazone ligand. The chromophores act electronically independently from each other, establishing the bichromophoric dyes as cassettes. Noteworthy, the scope of the ETC is not limited to the herein discussed examples, but could be expanded through the electronic fine-tuning of the charge-transfer properties of

the BASHY skeleton or the variation of the second chromophore. This structural flexibility of the photophysical engineering combined with the recently by us demonstrated site-selective bioconjugability of the BASHY platform[18] make this approach interesting for biotechnological applications. Further, the ETC compounds can be formulated in polymeric nanoparticles and used in bioimaging, as shown herein for dye **3**.

Experimental Section

Materials and Methods

All solvents and reagents for synthesis of the dyes and polymeric nanoparticles were purchased in the highest purity available and used as received. The salicylidenehydrazone ligand **1** and dye **5** were prepared according to previously by us reported procedures.[15] The boronic acid **2** and its pinacolate ester (**4**)[53] and the pinacolate ester of **6**[54] were prepared according to literature protocols. The ^{1}H NMR spectra were coincident with the published data. The pinacolate ester of **6** was converted into the free boronic acid intermediate by using a published method.[55] The product was used without further characterization for the synthesis of **7**. All NMR spectra were obtained in $CDCl_3$ on a Bruker Fourier 300 MHz instrument. The residual solvent signal (7.26 ppm for ^{1}H, 77.0 ppm for ^{13}C) was used as reference. Electrospray ionization (ESI) high-resolution mass spectra were measured with the aid of a QTRAP mass spectrometer.

Photophysical measurements were done at ambient temperature (23 °C) on air-equilibrated solutions of the dyes, contained in quartz cuvettes of 1-cm optical path length. A UV/vis absorption spectrometer (Shimadzu, UV-1603) and a fluorimeter (Varian Eclipse) with a pulsed Xenon lamp as excitation source were used. The excitation and emission spectra are corrected for the wavelength-dependent photomultiplier sensitivity. The emission quantum yields were measured with *N*-propyl-1,8-naphthalimide (Φ_{fluo} = 0.48 in acetonitrile)[15] or rhodamine B (Φ_{fluo} = 0.95 in ethanol)[56] as secondary or standard reference, respectively. The quantum yields are corrected for the differing refractive index of the solvent used for the sample and reference.

General Synthesis of Dyes 3 and 7

Stoichiometric amounts of ligand **1** and the corresponding boronic acid derivative **2** or **6** (both 0.1 mmol) were dissolved in 1 mL acetonitrile and stirred at 80 °C for 2 h in a round-bottom flask. Then the volatiles were evaporated and in the case of dye **3** the crude mixture was purified by silica-gel column chromatography using *n*-hexane/ethyl acetate (50/50) as eluent. Dye **7** was purified via filtration through a plug of silica, using ethyl acetate as eluent.

Dye **3**. Brownish-red amorphous solid, yield 30% (24 mg). ^{1}H NMR (300 MHz, $CDCl_3$): δ = 8.32 (s, 1H), 7.96–7.86 (m, 2H), 7.55–7.35 (m, 8H), 7.29–7.24 (m, 1H), 7.22–7.16 (m, 1H), 7.12–7.08 (m, 2H), 6.90–6.86 (m, 2H), 6.50 (s, 1H), 6.42 (dd, J = 9.3, 2.4 Hz, 1H), 6.27 (d, J = 2.4 Hz, 1H), 5.91 (s, 1H), 3.83 (s, 3H), 3.54–3.44 (m, 4H), 2.55 (s, 3H), 1.27 (s, 3H), 1.27–1.24 (m, 6H), 1.21 ppm (s, 3H); ^{13}C NMR (75 MHz, $CDCl_3$) δ = 161.5, 160.4, 157.5, 156.1, 154.8, 154.4, 153.6, 153.1, 142.9, 135.8, 134.8, 134.4, 132.6, 131.6, 131.1, 129.7, 129.5, 129.4, 129.1, 128.4, 127.2, 121.0, 117.3, 117.2, 114.3, 107.9, 106.1, 98.7, 55.5, 45.6, 29.8, 25.0, 14.6, 14.4, 12.9 ppm; HRMS (ESI) calcd for $C_{46}H_{43}O_4N_5B_2F_2Na$ $[M+Na]^+$: 812.3361; found: 812.3364.

Dye **7**. Orange amorphous solid, yield 63% (31 mg). ^{1}H NMR (300 MHz, $CDCl_3$): δ = 8.31 (s, 1H), 8.04–7.96 (m, 2H), 7.55 (d, J = 9.3 Hz, 1H), 7.46–7.30 (m, 6H), 7.25–7.21 (m, 1H), 6.34 (dd, J = 9.0, 2.1 Hz, 1H), 6.24 (d, J = 9.3 Hz, 1H), 6.15 (d, J = 2.1 Hz, 1H), 3.58–3.38 (m, 4H), 1.19 ppm (t, J = 7.5 Hz, 6H); ^{13}C NMR (75 MHz, $CDCl_3$): δ = 161.4, 157.6, 155.4, 153.7, 153.6, 143.7, 134.8, 132.4, 131.1, 129.43, 128.3, 127.1, 126.9, 118.7, 118.3, 115.9, 108.2, 106.3, 98.6, 45.5, 12.7 ppm; HRMS (ESI) calcd for $C_{28}H_{24}O_5N_3BNa$ $[M+Na]^+$: 516.1701; found: 516.1688.

Time-Dependent Density Functional Theory Calculations

All calculations were carried out using the Gaussian09 program.[57] The ground-state structures were geometry-optimized using density-functional-theory (DFT) with the CAM-B3LYP functional,[43] a 6-31G** basis set, and PCM for solvent (toluene) consideration.[44] No symmetry constraints were applied in the geometry optimizations and local energy minima were confirmed by the absence of imaginary frequencies. The vertical excitations of the optimized ground-state geometry were calculated with the time-dependent DFT (TD-DFT) method and the linear-response PCM; see Supporting Information.

Preparation of Polymeric Nanoparticles

Fluorescent plain PLGA-PVA nanoparticles were prepared using a double emulsion (*water-in-oil-in-water* (*w/o/w*)) solvent evaporation method, slightly modified with respect to a recent report.[47] Poly (lactic-co-glycolic acid) polymer (PLGA, lactide:glycolide 50:50, ester terminated, average molecular weight 7000–17000 g mol^{-1}, Aldrich) and 10 μg of dye **3** were dissolved in dichloromethane. An 8% (w/v) poly(vinyl alcohol) (PVA; average molecular weight 13000–23000 g mol^{-1}, Aldrich) aqueous solution was added and emulsified with the organic phase under continuous sonication at 20% of the amplitude for 15 s. A second emulsion was formed when this *w/o* emulsion was dispersed in a 2.5% (w/v) PVA aqueous solution under the same conditions. The *w/o/w* emulsion was poured drop wise into a 0.25% (w/v) PVA aqueous solution and stirred for 1 h at room temperature. The nanoparticles were washed with ultrapure water, collected by centrifugation (17500 rpm, 4 °C, 40 min), and finally re-suspended in sterile phosphate buffer saline (0.01 M, pH 7.4).

The mean nanoparticle size (Z-Average) and polydispersity index (PdI) were determined by dynamic light scattering (DLS, Malvern Instruments). The nanoparticle surface charge (zeta potential, ZP) was measured by laser Doppler electrophoresis (LDE) in combination with phase analysis light scattering (PALS) at 25 °C with the same equipment. The NP suspension (10 mg mL^{-1}) was diluted in 10 mM KCl to a final concentration of 0.6 mg mL^{-1}. All measurements were performed in triplicate.

Internalization Study and Dead Cell Evaluation

For the quantitative uptake study, murine immature bone marrow dendritic cells (BMDC; JAW SII, ATCC®CRL-11904™; ATCC, Manassas, VA, USA); 3.5×10^4 cells/190 μL/well) were seeded in 96-well plates and incubated overnight in a humidified incubator with 5% CO_2 at 37 °C, allowing the cells to become adherent. The cells were treated with fluorescent **3**-loaded PLGA NP (0.5 mg mL^{-1}) for 1, 3, and 18 h. The cells were then washed with sterile phosphate buffer saline (0.01 M, pH 7.4) and, if applicable, labeled with propidium iodide to evaluate the dead cell population. The medium and 0.05% (v/v) Triton X-100 were used as negative and positive controls, respectively. The fluorescence of 10000 cells was analyzed by flow

cytometry (LSR Fortessa cytometer; BD Biosciences) and data were treated with FlowJo software version 7.6.5 for Microsoft (TreeStar, San Carlos, CA, USA).

Confocal Fluorescence Microscopy

The fluorescent plain dye-loaded nanoparticles were added to previously seeded BMDC (6×10^4 cells/300 μL/well) and incubated for 2, 4, or 10 h. The cells were then fixed and co-stained with Hoechst 33342 (nucleus) and WGA-Alexa Fluor 633 (membrane). The images were obtained by confocal microscopy using an inverted microscope (Zeiss LSM 710; Carl Zeiss Microscopy GmbH) with a 63× oil (1.4 numerical aperture) plan-apochromat objective. Excitation of the fluorescent nanoparticles was performed using the 488 nm Ar ion laser line and the emission was collected at 550–600 nm. Excitation of WGA-Alexa Fluor 633 was performed using the 633 nm line from a HeNe laser. The excitation wavelength of Hoechst was set to 405 nm using a diode laser. The images were processed using ImageJ Software.

Statistical Analysis

Experimental results are expressed as mean ± standard deviation (SD). ANOVA and Tukey's post-hoc test were performed to demonstrate statistical differences ($p<0.05$), using the GraphPad Prism software (version 6) for Windows.

Acknowledgements

The financial support of the Portuguese Fundação para a Ciência e a Tecnologia (FCT) (grants SFRH/BD/94779/2013, PTDC/QEQ-QOR/1434/2014, PTDC/QEQ-MED/5512/2014, FEDER-029967, SAICTPAC/0019/2015, iMed.ULisboa grant UID/DTP/04138/2013, UTAP-ICDT/DTP-FTO/0016/2014, PhD fellowship PD/BD/113959/20 for A.I.M), the Spanish Ministerio de Ciencia, Innovación y Universidades (grants CTQ2014-54729-C2-1-P, CTQ2017-89832-P and PhD fellowship BES-2015-074458 for Z.D.), the Junta de Andalucía (P12-FQM-2140), the ERDF, and the Academy of Finland (decision 287954) is gratefully acknowledged. CSC–IT Center for Science Ltd, Finland is thanked for the allocation of computational resources.

Conflict of Interest

The authors declare no conflict of interest.

Keywords: energy transfer · fluorescence · hydrazones · organoboron · photophysics

[1] A. Dömling, W. Wang, K. Wang, *Chem. Rev.* **2012**, *112*, 3083–3135.
[2] S. Brauch, S. S. van Berkel, B. Westermann, *Chem. Soc. Rev.* **2013**, *42*, 4948–4962.
[3] C. Allais, J.-M. Grassot, J. Rodriguez, T. Constantieux, *Chem. Rev.* **2014**, *114*, 10829–10868.
[4] V. Estévez, M. Villacampa, J. C. Menéndez, *Chem. Soc. Rev.* **2014**, *43*, 4633–4657.
[5] L. Levi, T. J. J. Müller, *Chem. Soc. Rev.* **2016**, *45*, 2825–2846.
[6] L. Levi, T. J. J. Müller, *Eur. J. Org. Chem.* **2016**, 2907–2918.
[7] F. de Moliner, N. Kielland, R. Lavilla, M. Vendrell, *Angew. Chem. Int. Ed.* **2017**, *56*, 3758–3769; *Angew. Chem.* **2017**, *129*, 3812–3823.
[8] O. N. Burchak, L. Mugherli, M. Ostuni, J. J. Lacapère, M. Y. Balakirev, *J. Am. Chem. Soc.* **2011**, *133*, 10058–10061.
[9] A. Martorana, A. Pace, S. Buscemi, A. Palumbo Piccionello, *Org. Lett.* **2012**, *14*, 3240–3243.
[10] S. Brauch, M. Henze, B. Osswald, K. Naumann, L. A. Wessjohann, S. S. van Berkel, B. Westermann, *Org. Biomol. Chem.* **2012**, *10*, 958–965.
[11] A. Vázquez-Romero, N. Kielland, M. J. Arévalo, S. Preciado, R. J. Mellanby, Y. Feng, R. Lavilla, M. Vendrell, *J. Am. Chem. Soc.* **2013**, *135*, 16018–16021.
[12] L. Moni, C. F. Gers-Panther, M. Anselmo, T. J. J. Müller, R. Riva, *Chem. Eur. J.* **2016**, *22*, 2020–2031.
[13] S. T. A. Passos, J. R. Correa, S. L. M. Soares, W. A. Da Silva, B. A. D. Neto, *J. Org. Chem.* **2016**, *81*, 2646–2651.
[14] D. E. Ramírez-Ornelas, E. Alvarado-Martínez, J. Bañuelos, I. López-Arbeloa, T. Arbeloa, H. M. Mora-Montes, L. A. Pérez García, E. Peña-Cabrera, *J. Org. Chem.* **2016**, *81*, 2888–2898.
[15] F. M. F. Santos, J. N. Rosa, N. R. Candeias, C. Parente Carvalho, A. I. Matos, A. E. Ventura, H. F. Florindo, L. C. Silva, U. Pischel, P. M. P. Gois, *Chem. Eur. J.* **2016**, *22*, 1631–1637.
[16] A. D. Laurent, B. L. Guennic, D. Jacquemin, *Theor. Chem. Acc.* **2016**, *135*, 173.
[17] M. M. Alcaide, F. M. F. Santos, V. F. Pais, J. I. Carvalho, D. Collado, E. Pérez-Inestrosa, J. F. Arteaga, F. Boscá, P. M. P. Gois, U. Pischel, *J. Org. Chem.* **2017**, *82*, 7151–7158.
[18] P. M. S. D. Cal, F. Sieglitz, F. M. F. Santos, C. Parente Carvalho, A. Guerreiro, J. B. Bertoldo, U. Pischel, P. M. P. Gois, G. J. L. Bernardes, *Chem. Commun.* **2017**, *53*, 368–371.
[19] B. Zhang, G. Feng, S. Wang, X. Zhang, *Dyes Pigm.* **2017**, *149*, 356–362.
[20] C.-W. Wan, A. Burghart, J. Chen, F. Bergström, L. B.-Å. Johansson, M. F. Wolford, T. G. Kim, M. R. Topp, R. M. Hochstrasser, K. Burgess, *Chem. Eur. J.* **2003**, *9*, 4430–4441.
[21] R. Ziessel, C. Goze, G. Ulrich, M. Césario, P. Retailleau, A. Harriman, J. P. Rostron, *Chem. Eur. J.* **2005**, *11*, 7366–7378.
[22] A. Harriman, G. Izzet, R. Ziessel, *J. Am. Chem. Soc.* **2006**, *128*, 10868–10875.
[23] O. A. Bozdemir, Y. Cakmak, F. Sozmen, T. Ozdemir, A. Siemiarczuk, E. U. Akkaya, *Chem. Eur. J.* **2010**, *16*, 6346–6351.
[24] X. Qu, Q. Liu, X. Ji, H. Chen, Z. Zhou, Z. Shen, *Chem. Commun.* **2012**, *48*, 4600–4602.
[25] J. Fan, M. Hu, P. Zhan, X. Peng, *Chem. Soc. Rev.* **2013**, *42*, 29–43.
[26] L. D. Lavis, R. T. Raines, *ACS Chem. Biol.* **2014**, *9*, 855–866.
[27] G.-S. Jiao, L. H. Thoresen, T. G. Kim, W. C. Haaland, F. Gao, M. R. Topp, R. M. Hochstrasser, M. L. Metzker, K. Burgess, *Chem. Eur. J.* **2006**, *12*, 7816–7826.
[28] J. Han, A. Loudet, R. Barhoumi, R. C. Burghardt, K. Burgess, *J. Am. Chem. Soc.* **2009**, *131*, 1642–1643.
[29] L. Wu, A. Loudet, R. Barhoumi, R. C. Burghardt, K. Burgess, *J. Am. Chem. Soc.* **2009**, *131*, 9156–9157.
[30] D. Collado, P. Remón, Y. Vida, F. Nájera, P. Sen, U. Pischel, E. Pérez-Inestrosa, *Chem. Asian J.* **2014**, *9*, 797–804.
[31] Y. Xiao, D. Zhang, X. Qian, A. Costela, I. García-Moreno, V. Martín, M. E. Pérez-Ojeda, J. Bañuelos, L. Gartzia, I. López-Arbeloa, *Chem. Commun.* **2011**, *47*, 11513–11515.
[32] I. Esnal, G. Duran-Sampedro, A. R. Agarrabeitia, J. Bañuelos, I. García-Moreno, M. A. Macías, E. Peña-Cabrera, I. López-Arbeloa, S. de la Moya, M. J. Ortiz, *Phys. Chem. Chem. Phys.* **2015**, *17*, 8239–8247.
[33] X. Zhang, Y. Xiao, L. He, Y. Zhang, *J. Org. Chem.* **2014**, *79*, 6315–6320.
[34] S. Erbas-Cakmak, E. U. Akkaya, *Angew. Chem. Int. Ed.* **2013**, *52*, 11364–11368; *Angew. Chem.* **2013**, *125*, 11574–11578.
[35] S. Erbas-Cakmak, O. A. Bozdemir, Y. Cakmak, E. U. Akkaya, *Chem. Sci.* **2013**, *4*, 858–862.
[36] A. Loudet, K. Burgess, *Chem. Rev.* **2007**, *107*, 4891–4932.
[37] G. Ulrich, R. Ziessel, A. Harriman, *Angew. Chem. Int. Ed.* **2008**, *47*, 1184–1201; *Angew. Chem.* **2008**, *120*, 1202–1219.
[38] J. Mugnier, J. Pouget, J. Bourson, B. Valeur, *J. Lumin.* **1985**, *33*, 273–300.
[39] D. L. Dexter, *J. Chem. Phys.* **1953**, *21*, 836–850.
[40] S. Speiser, *Chem. Rev.* **1996**, *96*, 1953–1976.
[41] R. Ziessel, A. Harriman, *Chem. Commun.* **2011**, *47*, 611–631.
[42] T. Förster, *Ann. Phys.* **1948**, *2*, 55–75.
[43] T. Yanai, D. P. Tew, N. C. Handy, *Chem. Phys. Lett.* **2004**, *393*, 51–57.
[44] J. Tomasi, B. Mennucci, R. Cammi, *Chem. Rev.* **2005**, *105*, 2999–3094.

[45] Y. Zhao, Y. Zhang, X. Lv, Y. Liu, M. Chen, P. Wang, J. Liu, W. Guo, *J. Mater. Chem.* **2011**, *21*, 13168–13171.
[46] J. Jose, A. Loudet, Y. Ueno, L. Wu, H.-Y. Chen, D. H. Son, R. Barhoumi, R. Burghardt, K. Burgess, *Org. Biomol. Chem.* **2011**, *9*, 3871–3877.
[47] H. F. Florindo, S. Pandit, L. M. D. Gonçalves, M. Videira, O. Alpar, A. J. Almeida, *Biomaterials* **2009**, *30*, 5161–5169.
[48] W. Lin, L. Yuan, Z. Cao, Y. Feng, J. Song, *Angew. Chem. Int. Ed.* **2010**, *49*, 375–379; *Angew. Chem.* **2010**, *122*, 385–389.
[49] R. Goel, V. Luxami, K. Paul, *RSC Adv.* **2016**, *6*, 37664–37671.
[50] J. Zielonka, A. Sikora, J. Joseph, B. Kalyanaraman, *J. Biol. Chem.* **2010**, *285*, 14210–14216.
[51] G. Jones II, W. R. Jackson, C. Y. Choi, W. R. Bergmark, *J. Phys. Chem.* **1985**, *89*, 294–300.
[52] A. Takadate, T. Masuda, C. Murata, T. Tanaka, M. Irikura, S. Goya, *Anal. Sci.* **1995**, *11*, 97–101.
[53] J. Zhai, T. Pan, J. Zhu, Y. Xu, J. Chen, Y. Xie, Y. Qin, *Anal. Chem.* **2012**, *84*, 10214–10220.
[54] L. Du, M. Li, S. Zheng, B. Wang, *Tetrahedron Lett.* **2008**, *49*, 3045–3048.
[55] T. E. Pennington, C. Kardiman, C. A. Hutton, *Tetrahedron Lett.* **2004**, *45*, 6657–6660.
[56] R. F. Kubin, A. N. Fletcher, *J. Lumin.* **1982**, *27*, 455–462.
[57] Gaussian 09, Revision D.01, M. J. Frisch et al., Gaussian, Inc., Wallingford CT, **2013**.

Manuscript received: July 5, 2018
Version of record online: September 3, 2018